remote sensing

MDPI

Article

Landslide Susceptibility Mapping and Interpretation in the Upper Minjiang River Basin

Xin Wang [1] and Shibiao Bai [1,2,*]

[1] School of Marine Science and Engineering, Jiangsu Center for Collaborative Innovation in Geographical Information Resource Development and Application, Nanjing Normal University, Nanjing 210023, China
[2] China-Pakistan Joint Research Center on Earth Sciences, Institute of Mountain Hazards and Environment, Chinese Academy of Sciences, Chengdu 610041, China
* Correspondence: shibiaobai@njnu.edu.cn

Abstract: To enable the accurate assessment of landslide susceptibility in the upper reaches of the Minjiang River Basin, this research intends to spatially compare landslide susceptibility maps obtained from unclassified landslides directly and the spatial superposition of different types of landslide susceptibility map, and explore interpretability using cartographic principles of the two methods of map-making. This research using the catalogs of rainfall and seismic landslides selected nine background factors those affect the occurrence of landslides through correlation analysis finally, including lithology, NDVI, elevation, slope, aspect, profile curve, curvature, land use, and distance to faults, to assess rainfall and seismic landslide susceptibility, respectively, by using a WOE-RF coupling model. Then, an evaluation of landslide susceptibility was conducted by merging rainfall and seismic landslides into a dataset that does not distinguish types of landslides; a comparison was also made between the landslide susceptibility maps obtained through the superposition of rainfall and seismic landslide susceptibility maps and unclassified landslides. Finally, confusion matrix and ROC curve were used to verify the accuracy of the model. It was found that the accuracy of the training set, testing set, and the entire data set based on the WOE-RF model for predicting rainfall landslides were 0.9248, 0.8317, and 0.9347, and the AUC area were 1, 0.949, and 0.955; the accuracy of the training set, testing set, and the entire data set for seismic landslides prediction were 0.9498, 0.9067, and 0.8329, and the AUC area were 1, 0.981, and 0.921; the accuracy of the training set, testing set, and the entire data set for unclassified landslides prediction were 0.9446, 0.9080, and 0.8352, and the AUC area were 0.9997, 0.9822, and 0.9207. Both of the confusion matrix and the ROC curve indicated that the accuracy of the coupling model is high. The southeast of the line from Mount Xuebaoding to Lixian County is a high landslide prone area, and through the maps, it was found that the extremely high susceptibility area of seismic landslides is located at a higher elevation than rainfall landslides by extracting the extremely high susceptibility zones of both. It was also found that the results of the two methods of evaluating landslide susceptibility were significantly different. As for a same background factor, the distribution of the areas occupied by the same landslide occurrence class was not the same according to the two methods, which indicates the necessity of conducting relevant research on distinguishing landslide types.

Keywords: background factors; landslide susceptibility; WOE-RF; rainfall landslide; seismic landslide; space comparison

Citation: Wang, X.; Bai, S. Landslide Susceptibility Mapping and Interpretation in the Upper Minjiang River Basin. *Remote Sens.* **2023**, *15*, 4947. https://doi.org/10.3390/rs15204947

Academic Editor: Alex Hay-Man Ng

Received: 12 July 2023
Revised: 4 October 2023
Accepted: 8 October 2023
Published: 13 October 2023

1. Introduction

China is one of the countries where geological hazards such as landslides, avalanches, and mudslides occur frequently; geological hazards generally cause serious human and socio-economic losses. The exploration of the spatial relationship between geological hazards and occurrence factors can reduce the risk of geological hazards to a certain extent. Landslide hazard susceptibility is the answer to the question of where landslides are likely

to occur in space, and it aims to establish the relationship between landslides and the factors that affect landslide occurrence and evaluate the regional landslide hazard susceptibility based on this relationship [1–3].

Canadian geologist Agterberg proposed the weight of evidence model based on the GIS platform [4–6]; Dahal et al., 2008 [7] explored the weight of evidence approach in the evaluation of the landslide susceptibility of small watersheds using two small watersheds in Shikoku, Japan as the study area; Sadisun et al., 2021 [8] used Sigi Biromaru as the study area to undertake a landslide susceptibility evaluation based on the weight of evidence model; and Yang et al., 2020 [9] and Hu et al., 2020 [10] evaluated the landslide susceptibility of Jiuzhaigou and Badong County based on the weight of evidence method, respectively, and the studies all showed that the accuracy of the model was high, and then many scholars improved and applied it based on the common weight of evidence method [7,8,11,12]. With the development of spatial–temporal data mining, machine learning has also been gradually applied to the evaluation of geological hazards by scholars. Bai et al., 2011 [13] studied the landslide susceptibility of Lianyungang city in China using a rare event logistic regression model in 2011; Mao et al., 2015 [14] found that, compared with plain Bayesian, uncertainty-based Bayesian classification in evaluating the landslide hazard in Baota district of Yan'an city could better reflect the landslide hazard development characteristics; Wang et al., 2021 [15] carried out a landslide susceptibility evaluation in Jingzhou County, Hunan Province using an SVM algorithm. The random forest model is a popular model for landslide susceptibility evaluation that is less sensitive to noise and outliers, less prone to overfitting, more inclusive of data imbalance, and more stable in prediction [16,17]. Wu et al., 2017 [18] evaluated the landslide hazard in the Dongjiang Basin based on the random forest model; Liu et al., 2018 [19] evaluated the landslide susceptibility in Sha and Xi township–Xeitan township in the Three Gorges reservoir area using a random forest model. Gradually, deep learning has also been applied to predict the susceptibility of hazards such as landslides owing to its superiority. Mandal et al., 2021 used a CNN convolutional neural network to predict the landslide susceptibility of Rorachu river basin [20]; and Wang et al., 2023 used a deep learning algorithm to predict the landslide susceptibility of the Jiuzhaigou area [21]. But deep learning algorithms are often implicit in the expression of knowledge structures, so they have the disadvantage of difficult interpretability.

The coupling of multiple models for landslide susceptibility evaluation is currently receiving more and more attention. Arabameri et al., 2019 evaluated landslide susceptibility in the Gorganroud watershed of northern Iran using the LNRF-LMR coupled model [22]; Pourghasemi et al., 2019 evaluated the susceptibility of flood and landslide hazards in the Lorestan province of Iran using a SWARA-ANFIS-Gray wolf coupled model, respectively [23]; Guo et al., 2019 [24] evaluated the landslide susceptibility of the Wanzhou district in the Three Gorges reservoir area based on a coupled model of weight of evidence and a BP neural network; Li et al., 2021 [25] coupled an information quantity model with a logistic regression model to predict landslide susceptibility in Chongyi county, Jiangxi province; Ma et al., 2022 [26] used a coupled random forest-frequency ratio model to evaluate the landslide susceptibility in Lueyang County, which improved the accuracy by 10.7% and 4.9%, respectively, compared with the two single models; Bai et al., 2022 [27] evaluated the landslide susceptibility in the northeast of Yu based on the entropy index and a random forest coupled model, and the studies all showed that the coupled model has a higher prediction accuracy than the single prediction model.

The multi-hazard direction in hazard science research is one of the hotspots at home and abroad [28–33], but, at present, the whole is still dominated by single hazard research. In terms of the susceptibility mapping of hazards, a large number of studies have also mapped the susceptibility of single hazards, such as landslides, floods, forest fires, etc., due to the differences in the background and triggering factors of each hazard [34–36] and, among the methods used to span the spatial susceptibility from a single hazard to a multi-hazard, the spatial superposition of single hazards has mainly been used [23]. From the big concept of hazards to the small concept of landslides, the same background

factor or triggering factor has different impacts on the development of different types of landslides, so when mapping the landslide susceptibility of a certain area, different landslide catalogs should also be used as input. Currently, some scholars have also carried out studies to distinguish landslide types with different trigger factors: Wang et al., 2012 analyzed the causal mechanism of landslide hazards triggered by rainfall and earthquakes through physical simulation experiments [37]; Ding 2013 used suitable models to study the mechanisms of landslides under earthquakes and rainfall [38]; Bai et al., 2013 used a logistic regression model to separately assess rainfall and seismic landslide susceptibility; and the necessity of separating rainfall and seismic landslides was also proposed through related studies [39]. In this research, we propose to evaluate the landslide susceptibility of the upper reaches of the Minjiang River Basin by using different mapping principles and using both unclassified and classified types of landslides, respectively.

At present, there has been relatively little research on the classification of rainfall and seismic landslides in the upper reaches of the Minjiang River Basin conducted by predecessors. Therefore, the susceptibility mapping of the two types of landslides is lacking, making it difficult to provide sufficient support for the prevention and control of landslide geological disasters. This research intends to take the upper reaches of the Minjiang River Basin as an example to obtain evaluation maps of rainfall, seismic, and unclassified landslide susceptibility, respectively. The development patterns of different types of landslides based on background factors will be explored at the same time. Meanwhile, this research proposes to refer to the spatial superposition of multiple hazards [40], obtaining spatial comparisons of landslide susceptibility maps obtained from unclassified landslides and the final landslide susceptibility map obtained by overlaying rainfall and seismic landslide susceptibility maps, and it also attempts to explain the variability in spatial distribution in terms of cartographic principles. In addition, this research combines the weight of evidence with the random forest algorithm. The reason for coupling the weight of evidence with the random forest model is that this research mainly investigates the effect of different landslide catalogs on the prediction results of compound landslide susceptibility (i.e., spatial superposition of rainfall and seismic landslide susceptibility maps to obtain the compound landslide susceptibility map, and susceptibility map obtained by using unclassified landslides), and attempts to explain the two results in terms of the mapping principle in order to help elucidate the need to use different landslide catalogs for different problems. The contribution of different cataloged landslides to each background factor is different since the two methods use different landslide catalogs, which makes the spatial relationship between landslides and background factors not the same, so it is necessary to firstly get the spatial relationship to derive the contribution of each background factor to the landslide prediction, as opposed to directly inputting the values of the background factors into the model for prediction. The coupling of the two models can make the prediction results more realistic.

2. Study Area

The upper Minjiang River Basin is located in the eastern margin of the Tibetan Plateau, covering an area of about 22,000 km^2 [41], and its elevation changes are between 694 and 5840 m. The geological structure is complex, mainly composed of NE- and NW-oriented faults, with frequent seismic activity [42]. The stratigraphic lithology is dominated by sandstones and siltstones interspersed with micaceous rocks; shales, micaceous, and siltstones; limestones and sandstones; and granitic rocks. It is also influenced by the southwest monsoon, with rainfall concentrated in summer, and it experiences serious effects of geological hazards such as landslides. The region is similar to other regions located on the Tibetan Plateau, with the same active environmental conditions and more intense climate change [43]. The upper reaches of the Minjiang River Basin studied in this research mainly include Songpan, Maoxian, Lixian, Wenchuanxian, and Dujiangyan where several major cities are located, and 3343 landslide sites were collected here, including

407 rainfall landslides and 2936 seismic landslides. The catalogued data of landslides used in this research and the overview of the study area are shown in Figure 1.

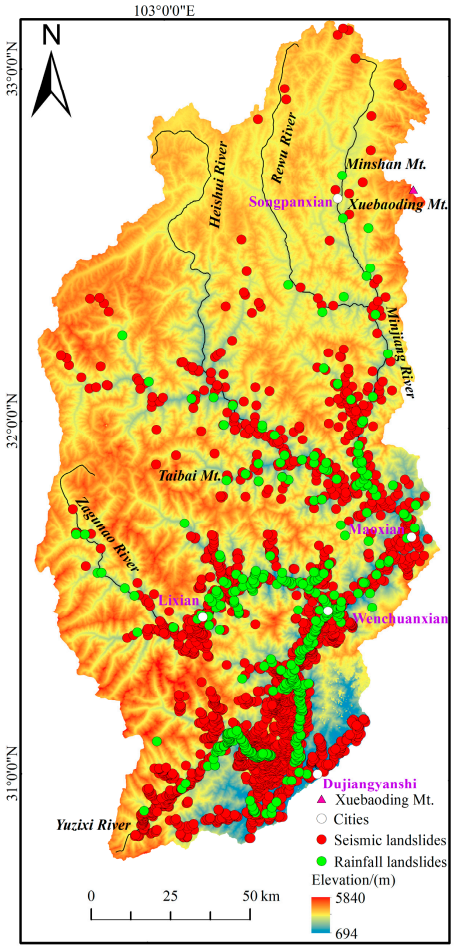

Figure 1. Overview of the study area.

3. Research Data and Methods

3.1. Data

This study used the inventory data of rainfall and seismic landslide point sites in the upper reaches of the Minjiang River Basin, as well as background factors related to the occurrence of two types of landslides. The specific data and sources are shown in Table 1:

Table 1. Data sources for spatial susceptibility assessment of landslides in the upper reaches of Minjiang River Basin.

Data	Source
Rainfall landslides	Ministry of Land and Resources of China: Survey and mapping of 1:100,000 landslides in China from 1999 to 2008 [41]
Seismic landslides	Ministry of Land and Resources of China: Investigation of Landslide Hazard Caused by 2008 Wenchuan Earthquake in China [41]
Factors related to landslide occurrence	DTM image with 90 m spatial resolution [41]
NDVI	Resource and environmental science data registration and publishing system [44]

Among the data we used in this research, the rainfall landslides were obtained from the 1:100,000 landslide hazard survey and mapping of China from 1999 to 2008 by the Ministry of Land and Resources of China, and there were 407 rainfall landslide point sites; the seismic landslides were obtained from the Ministry of Land and Resources of China. According to the investigation of landslide disasters caused by the 2008 Wenchuan earthquake, there were a total of 2936 landslide point sites. From Figure 1, it can be seen that landslide point sites were roughly distributed along the main stream of the Minjiang River and its tributaries. The geologic background factors related to the occurrence of landslides (such as slope, slope direction, etc.) were extracted from DTM images with 90 m spatial resolution. The NDVI index data related to the occurrence of landslides were obtained from the year-by-year NDVI maximum dataset of China with 30 m spatial resolution released by Xu Xinliang in the Resource and Environmental Science Data Registration and Publication System.

3.2. Study Methods

3.2.1. Weight of Evidence Model

Taking landslide as an example, weight of evidence method is a data-driven model based on the uncertainty of probability and Bayes' law to find the posterior probability of landslide occurrence by spatially superimposing the evidence factors assigned weights based on exploring the spatial correlation between landslides and the evidence factors affecting landslide occurrence.

The basic principle is as follows [45,46]: Suppose there are m landslide point sites in the study area. Firstly, the study area is spatially divided into a grid according to a certain scale, and there is only one landslide point site in each grid, then, the priori probability of landslide occurrence in the study area is (m/a), and n_1, n_2, n_3, etc. are n geological factors related to landslide occurrence. Choose the jth geological factor, make n_j that a geological factor exists and $\neg n_j$ that a geological factor does not exist, then overlay the landslide layer with the geological factor n_j layer to obtain 4 cases of $n_j \cap m$, $\neg n_j \cap m$, $n_j \cap \neg m$, and $\neg n_j \cap \neg m$, and the following 4 conditional probabilities can be defined based on these:

$$P\left(m|n_j\right) = \frac{n_j \cap m}{n_j} \tag{1}$$

$$P\left(\neg m|n_j\right) = \frac{n_j \cap \neg m}{n_j} \tag{2}$$

$$P\left(m|\neg n_j\right) = \frac{\neg n_j \cap m}{\neg n_j} \tag{3}$$

$$P\left(\neg m|\neg n_j\right) = \frac{\neg n_j \cap \neg m}{\neg n_j} \tag{4}$$

Based on the above four conditional probability formulas, the Bayes' law yields the following:

$$P\left(m|\neg n_j\right) = \frac{P\left(\neg n_j|m\right)P(m)}{P\left(\neg n_j\right)} \tag{5}$$

The *j*th evidence layer has positive weight W_j^+ and negative weight W_j^-, respectively, and is taken as W_j^+ when n_j exists and W_j^- when n_j does not exist:

$$W_j^+ = \ln\frac{P(n_j|m)}{P(n_j|\neg m)} \tag{6}$$

$$W_j^- = \ln\frac{P(\neg n_j|m)}{P(\neg n_j|\neg m)} \tag{7}$$

This leads to a relationship between the evidence power of the n_j layer and the likelihood ratio and conditional ratio of the occurrence of landslides, which is expressed as the evidence power in the form of

$$W_j^+ = \ln\left(\frac{O\left(m|n_j\right)}{O(m)}\right) \tag{8}$$

$$W_j^- = \ln\left(\frac{O\left(m|\neg n_j\right)}{O(m)}\right) \tag{9}$$

In this research, we obtain the total weight W of the evidence factors by finding each evidence factor W_j^+ and W_j^- based on the SDM toolbox developed on Arcgis platform.

3.2.2. Random Forest Model

Breiman [47] proposed random forest as an integrated method in 2001. The sampling method used in random forest is bootstrap resampling, and its randomness lies in the random sampling of the feature factors and the number of samples. Then, decision trees are used to model each bootstrap sample based on the extracted samples. When modeling the random forest, the number of decision trees ultimately used to construct the random forest can be determined by the trend of the model's error variation. The decision trees are independent of each other, and each one of them yields a classification result; the final classification result is obtained by the result of the plurality of all decision trees.

The construction of a decision tree often goes through 3 processes: feature selection, decision tree generation, and decision tree pruning. The selection of features is based on the information gain. The information gain of feature factor n_j on dataset d is denoted as $g\left(d, n_j\right)$, which is the difference between the empirical entropy H (d) of dataset d and the empirical conditional entropy of d under the given condition of feature factor n_j [48].

Suppose X is a discrete random variable taking finite values with probability distribution $P(X = x_i) = p_i$, I = 1, 2, …, n, then the entropy of the random variable X is as follows:

$$H(X) = -\sum_{i=1}^{n} p_i \log p_i \tag{10}$$

Suppose the random variable (X, Y) with joint probability distribution $P(X = x_i, Y = y_i) = p_{ij}$, i = 1, 2, …, n; j = 1, 2, …, m, then the conditional entropy is as follows:

$$H(Y \mid X) = \sum_{i=1}^{n} p_i H(Y \mid X = x_i) \tag{11}$$

where $p_i = P(X = x_i)$, i = 1, 2, …, n.

Then, the information gain of feature factor n_j on dataset D is noted as follows:

$$g(D, n_j) = H(D) - H(D \mid n_j) \tag{12}$$

The criterion for decision tree generation is to select the feature factors with the greatest information gain in order from the root node for the construction of root and leaf nodes. To improve the generalization ability of the model, the generated decision tree also needs to be pruned.

3.2.3. WOE-RF Model

The weight value calculated in the WOE model is an expression of the spatial relationship between the factors affecting the occurrence of landslides and landslides. By calculating the weight of factors on landslides, the secondary factors with similar effects on landslides can be grouped into one category based on the weight value, which can reduce the redundancy of the input data of machine learning models and improve the accuracy of machine learning to a certain extent. Figure 2 shows the schematic diagram of the application of the combination of the weight of evidence and the random forest model.

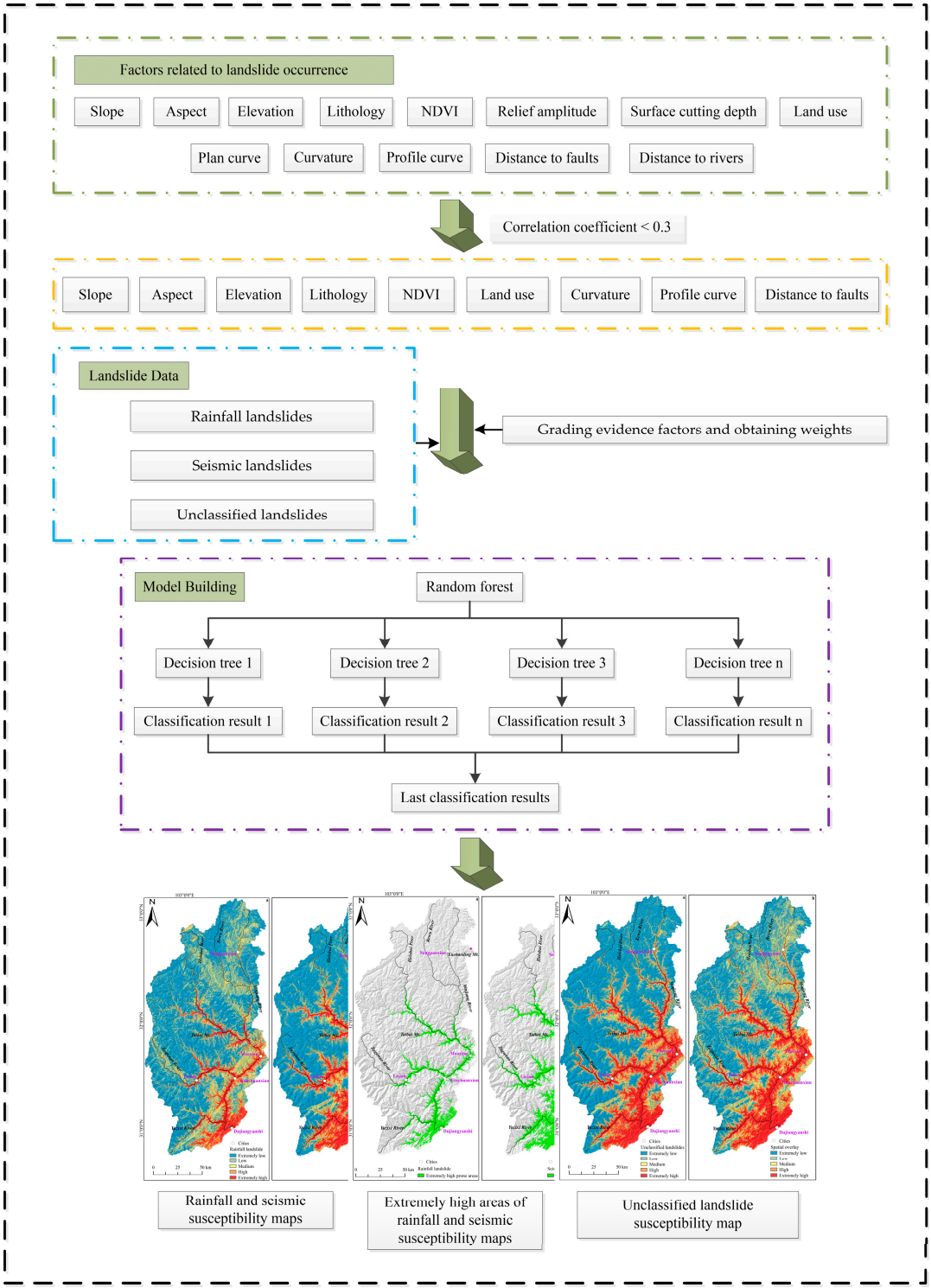

Figure 2. The Flow Chart of WOE-RF Coupling Model Application.

3.2.4. Accuracy Validation of WOE-RF Model

In this research, the confusion matrix [49] and the ROC curve [50] are used to validate the accuracy of the WOF-RF model.

Through the confusion matrix, we can obtain four cases: actual landslide and predicted landslide (TP), actual not landslide and predicted not landslide (TN), actual landslide but

predicted not landslide (FN), and actual not landslide but predicted landslide (FP), from which we can obtain the model prediction accuracy and recall based on the formula:

$$\text{Accuracy} = \frac{\text{TP} + \text{TN}}{\text{TP} + \text{TN} + \text{FN} + \text{FP}} \tag{13}$$

$$\text{Recall} = \frac{\text{TP}}{\text{TP} + \text{FN}} \tag{14}$$

The accuracy of the model was also evaluated by AUC area under the ROC curve, with the horizontal axis of the ROC curve representing false positives and the vertical axis representing true positives. Generally, the larger the AUC area under the ROC curve, the higher the accuracy is indicated. The above two ways of evaluating the prediction accuracy of the model can roughly assess the applicability of the model.

3.2.5. Landslide Susceptibility Classification

The obtained landslide susceptibility maps of rainfall, seismic, and unclassified landslide in the upper Minjiang River Basin were classified based on natural intermittent points [10,51], and the natural intermittent point method can be able to make the smallest differences within the classified classes and the largest differences between classes. Since the landslide and non-landslide threshold in this research was set to 0.9, the value of class 5 will be changed to [0.9, 1] on the basis of the natural interruption point classification.

4. Results

4.1. Landslide Background Factors Pretreatment

Considering the area of the upper reaches of the Minjiang River Basin, the distribution of landslides, and the accuracy of the original topography, this research chose to establish a 200 × 200 m grid for analysis, and initially selected lithology, NDVI, elevation, slope, aspect, relief amplitude, surface cutting depth, profile curve, plan curve, curvature, land use, distance to faults, and distance to rivers for analysis, which are the 13 most relevant background factors to the landslides in the upper reaches of Minjiang River Basin. Among them, two linear elements of faults as well as rivers were buffered at 200 m intervals throughout the whole study area, and correlation analysis was performed for the 13 selected factors, then correlation coefficients that were less than 0.3 were considered uncorrelated between the factors [52]; finally, there were nine background factors involved in the model building through correlation analysis. The nine landslide susceptibility modeling background factors included the following: lithology, NDVI, elevation, slope, aspect, profile curve, curvature, land use, and distance to faults. Among them, the two discrete variables of lithology and land use by category were renumbered; the aspects were divided into nine categories according to the values, where -1 was divided into plane, (0, 22.5) and (337.5, 360) for north, (22.5, 67.5) for northeast, (67.5, 112.5) for east, (112.5, 157.5) for southeast, (157.5, 202.5) for south, (202.5, 247.5) for southwest, (247.5, 292.5) for west, and (292.5, 337.5) for northwest; the remaining continuous type factors were divided into equal intervals according to the distribution of the data. The specific factor grades are shown in Figure 3.

4.2. Acquisition of Weights for Landslide Background Factors

Based on the nine landslide background factors of lithology, NDVI, elevation, slope, aspect, profile curve, curvature, land use, and distance to faults, the factor weights of rainfall, seismic, and unclassified landslides were obtained after grading; the weights of the nine factors are as shown in Tables 2–4, respectively:

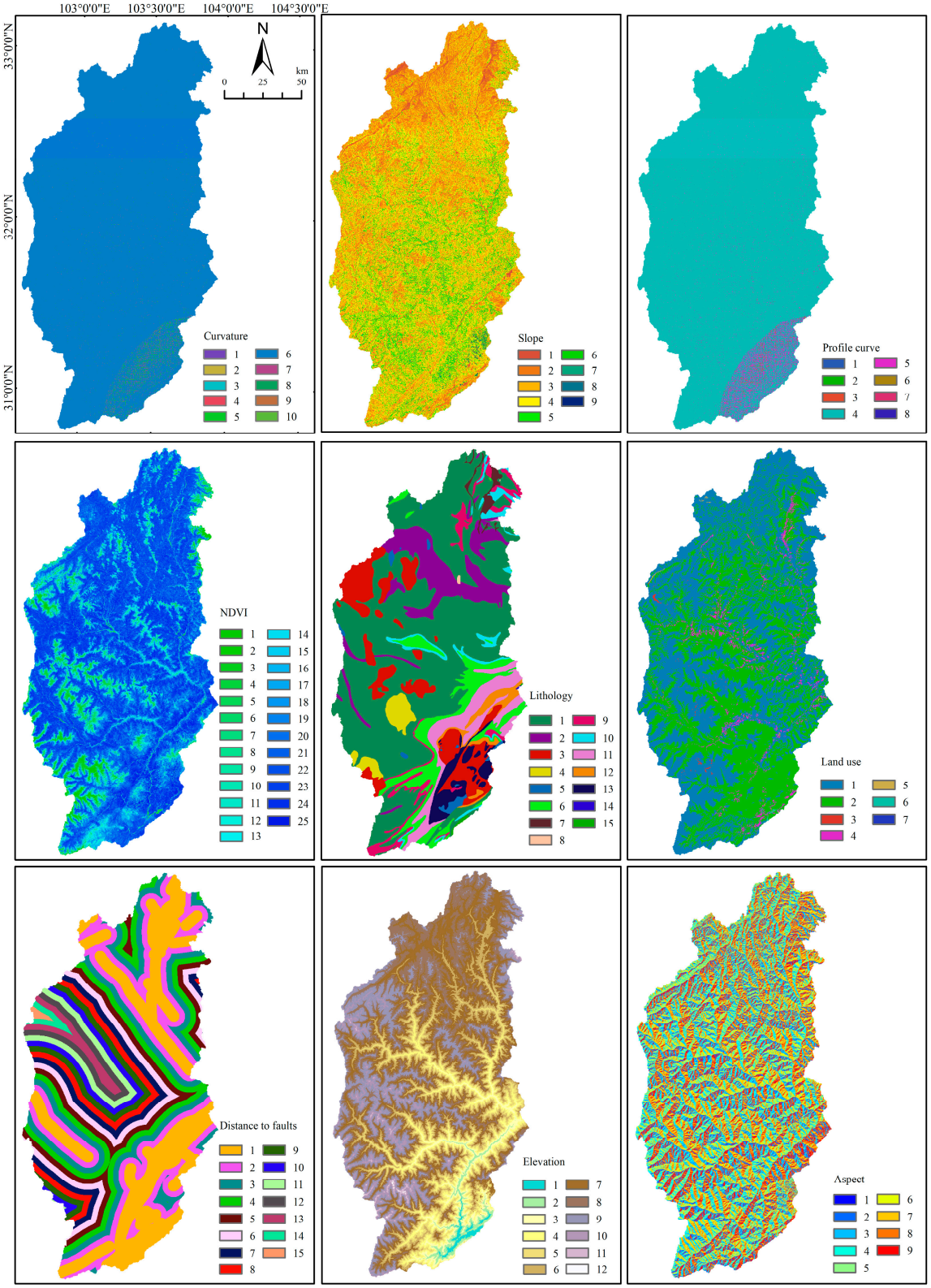

Figure 3. Classification of landslide background factors in the upper reaches of Minjiang River Basin.

Table 2. Weight value of rainfall landslides background factors.

Evidence Factors	Classification of Factors	Weight			
Aspect			Lithology		
Flat	1	0.0007	Sandstone, siltstone interbedded with phyllite	1	−0.9971
N	2	−0.6819	Shale, phyllite, and siltstone	2	−1.7158
NE	3	0.0007	Granitic rocks	3	−0.1886
E	4	0.0007	Syenite	4	−0.1886
SE	5	0.3216	Diorite	5	1.4918
S	6	0.0007	Limestone and sandstone	6	0.8567
SW	7	0.0007	Unconsolidated deposits	7	−0.1886
W	8	0.0007	Sandstone, siltstone, and shale	8	−0.1886
NW	9	0.0007	Limestone intercalated with shale	9	0.5665
NDVI			Limestone, sandstone, and shale	10	−0.1886
(46, 396.9)	1	−0.1110	Limestone and dolomite intercalated with phyllite	11	0.9109
(396.9, 747.8)	2	−0.1110	Dolomite, silicalite, phyllite, sandstone, and siltstone	12	0.7918
(747.8, 1098.8)	3	−0.1110	Amphibolite	13	1.8850
(1098.8, 1449.7)	4	−0.1110	Sandstone and siltstone intercalated with slate	14	−0.1886
(1449.7, 1800.6)	5	−0.1110	Sandstone and siltstone interbedded with shale	15	−0.1886
(1800.6, 2151.5)	6	−0.1110	Profile curve		
(2151.5, 2502.4)	7	−0.1110	(−38.6, −28.6)	1	−1.6067
(2502.4, 2853.4)	8	1.0049	(−28.6, −18.6)	2	−1.6067
(2853.4, 3204.3)	9	0.8565	(−18.6, −8.6)	3	2.0356
(3204.3, 3555.2)	10	0.8724	(−8.6, 2.6)	4	−0.0839
(3555.2, 3906.1)	11	−0.1110	(2.6, 12.6)	5	0.8969
(3906.1, 4257.0)	12	−0.1110	(12.6, 22.6)	6	2.3935
(4257.0, 4608.0)	13	0.7309	(22.6, 32.6)	7	−1.6067
(4608.0, 4958.9)	14	0.7546	(32.6, 44.3)	8	−1.6067
(4958.9, 5309.8)	15	−0.1110	Curvature		
(5309.8, 5660.7)	16	−0.1110	(−87, −71)	1	−2.0171
(5660.7, 6011.6)	17	−0.1110	(−71, −55)	2	−2.0171
(6011.6, 6362.6)	18	0.4277	(−55, −39)	3	−2.0171
(6362.6, 6713.5)	19	−0.1110	(−39, −23)	4	−2.0171
(6713.5, 7064.4)	20	−0.1110	(−23, −7)	5	1.1956
(7064.4, 7415.3)	21	−0.1110	(−7, 9)	6	−0.0528
(7415.3, 7766.2)	22	−0.2762	(9, 26)	7	1.5568
(7766.2, 8117.2)	23	−0.2694	(26, 42)	8	−2.0171
(8117.2, 8468.1)	24	−0.1110	(42, 58)	9	−2.0171
(8468.1, 8819.0)	25	0.7211	(58, 73)	10	−2.0171

Table 2. *Cont.*

Evidence Factors	Classification of Factors	Weight			
Elevation			Land use		
(712.0, 1132.5)	1	2.7367	Garden plot	1	−0.5322
(1132.5, 1553.0)	2	2.9041	Woodland	2	0.1154
(1553.0, 1973.5)	3	2.2586	Land for water bodies and water conservancy facilities	3	−4.4595
(1973.5, 2394.0)	4	1.0646	Grassland	4	1.7991
(2394.0, 2814.5)	5	−1.7875	Commercial area	5	3.0203
(2814.5, 3235.0)	6	−1.3411	Land for industrial and mining warehousing	6	−4.4595
(3235.0, 3655.5)	7	−2.9547	Other land	7	−4.4595
(3655.5, 4076.0)	8	−1.7875	Distance to faults		
(4076.0, 4496.5)	9	−1.7875	(0, 17.8)	1	0.6291
(4496.5, 4917.0)	10	−2.8276	(17.8, 35.6)	2	0.4427
(4917.0, 5337.5)	11	−1.7875	(35.6, 53.4)	3	−0.7052
(5337.5, 5758.0)	12	−1.7875	(53.4, 71.2)	4	−0.3361
Slope			(71.2, 89.0)	5	−0.3361
(0, 10)	1	0.9478	(89.0, 106.8)	6	−1.1051
(10, 20)	2	−0.6397	(106.8, 124.6)	7	−0.8145
(20, 30)	3	−0.3065	(124.6, 142.4)	8	−1.4800
(30, 40)	4	−0.1079	(142.4, 160.2)	9	−1.1470
(40, 50)	5	0.3697	(160.2, 178)	10	−1.8685
(50, 60)	6	0.7293	(178, 195.8)	11	−1.0934
(60, 70)	7	1.3741	(195.8, 213.6)	12	−1.0272
(70, 80)	8	−0.1079	(213.6, 231.4)	13	−0.3361
(80, 90)	9	−0.1079	(231.4, 249.2)	14	−0.3361
			(249.2, 267.0)	15	−0.3361

Table 3. Weight value of seismic landslides background factors.

Evidence Factors	Classification of Factors	Weight			
Aspect			Lithology		
Flat	1	−0.0223	Sandstone, siltstone interbedded with phyllite	1	−0.7654
N	2	−0.0223	Shale, phyllite, and siltstone	2	−2.2745
NE	3	−0.0223	Granitic rocks	3	0.1397
E	4	0.2072	Syenite	4	−2.7594
SE	5	0.2476	Diorite	5	1.6636
S	6	0.1265	Limestone and sandstone	6	0.4612
SW	7	−0.1626	Unconsolidated deposits	7	−3.2859
W	8	−0.3399	Sandstone, siltstone, and shale	8	0.0117
NW	9	−0.2294	Limestone intercalated with shale	9	0.0117

Table 3. *Cont.*

Evidence Factors	Classification of Factors	Weight			
NDVI			Limestone, sandstone, and shale	10	0.0117
(46, 396.9)	1	0.0249	Limestone and dolomite intercalated with phyllite	11	0.7738
(396.9, 747.8)	2	0.0249	Dolomite, silicalite, phyllite, sandstone, and siltstone	12	1.0732
(747.8, 1098.8)	3	−3.2095	Amphibolite	13	2.0384
(1098.8, 1449.7)	4	−2.3885	Sandstone and siltstone intercalated with slate	14	0.0117
(1449.7, 1800.6)	5	−1.2734	Sandstone and siltstone interbedded with shale	15	0.0117
(1800.6, 2151.5)	6	−0.9951	Profile curve		
(2151.5, 2502.4)	7	−0.5969	(−38.6, −28.6)	1	1.0324
(2502.4, 2853.4)	8	0.0249	(−28.6, −18.6)	2	1.0324
(2853.4, 3204.3)	9	0.0249	(−18.6, −8.6)	3	2.0926
(3204.3, 3555.2)	10	0.0249	(−8.6, 2.6)	4	−0.1531
(3555.2, 3906.1)	11	0.0249	(2.6, 12.6)	5	1.4408
(3906.1, 4257.0)	12	0.0249	(12.6, 22.6)	6	2.3560
(4257.0, 4608.0)	13	0.3107	(22.6, 32.6)	7	1.0324
(4608.0, 4958.9)	14	0.2456	(32.6, 44.3)	8	1.0324
(4958.9, 5309.8)	15	0.0249	Curvature		
(5309.8, 5660.7)	16	0.4826	(−87, −71)	1	0.6172
(5660.7, 6011.6)	17	0.2905	(−71, −55)	2	0.6172
(6011.6, 6362.6)	18	0.1779	(−55, −39)	3	0.6172
(6362.6, 6713.5)	19	0.2509	(−39, −23)	4	0.6172
(6713.5, 7064.4)	20	0.0249	(−23, −7)	5	1.5330
(7064.4, 7415.3)	21	0.0249	(−7, 9)	6	−0.0776
(7415.3, 7766.2)	22	−0.2809	(9, 26)	7	1.8013
(7766.2, 8117.2)	23	−0.1779	(26, 42)	8	0.6172
(8117.2, 8468.1)	24	0.1977	(42, 58)	9	0.6172
(8468.1, 8819.0)	25	0.7341	(58, 73)	10	0.6172
Elevation			Land use		
(712.0, 1132.5)	1	2.2752	Garden plot	1	−0.6334
(1132.5, 1553.0)	2	2.5161	Woodland	2	0.3175
(1553.0, 1973.5)	3	1.9906	Land for water bodies and water conservancy facilities	3	−1.1400
(1973.5, 2394.0)	4	1.3606	Grassland	4	1.2023
(2394.0, 2814.5)	5	0.5051	Commercial area	5	1.0398
(2814.5, 3235.0)	6	−0.4698	Land for industrial and mining warehousing	6	−1.1400
(3235.0, 3655.5)	7	−1.6533	Other land	7	−1.1400
(3655.5, 4076.0)	8	−2.7238	Distance to faults		
(4076.0, 4496.5)	9	−4.4023	(0, 17.8)	1	0.8153
(4496.5, 4917.0)	10	−3.7094	(17.8, 35.6)	2	0.1081
(4917.0, 5337.5)	11	−7.3573	(35.6, 53.4)	3	−0.5102
(5337.5, 5758.0)	12	−7.3573	(53.4, 71.2)	4	−0.3852

Table 3. *Cont.*

Evidence Factors	Classification of Factors	Weight			
Slope			(71.2, 89.0)	5	−0.5233
(0, 10)	1	−0.1749	(89.0, 106.8)	6	−0.6628
(10, 20)	2	−0.7377	(106.8, 124.6)	7	−1.2068
(20, 30)	3	−0.5357	(124.6, 142.4)	8	−1.8504
(30, 40)	4	0.0610	(142.4, 160.2)	9	−1.3686
(40, 50)	5	0.6785	(160.2, 178)	10	−1.1733
(50, 60)	6	1.0211	(178, 195.8)	11	−1.2810
(60, 70)	7	1.0880	(195.8, 213.6)	12	−1.7543
(70, 80)	8	1.5884	(213.6, 231.4)	13	−2.2307
(80, 90)	9	0.8379	(231.4, 249.2)	14	−7.9980
			(249.2, 267.0)	15	−7.9980

Table 4. Weight value of unclassified landslides background factors.

Evidence Factors	Classification of Factors	Weight			
Aspect			Lithology		
Flat	1	0.0331	Sandstone, siltstone interbedded with phyllite	1	−0.7916
N	2	−0.1245	Shale, phyllite, and siltstone	2	−2.1887
NE	3	0.0331	Granitic rocks	3	0.1404
E	4	0.1680	Syenite	4	−2.8900
SE	5	0.2614	Diorite	5	1.6488
S	6	0.0981	Limestone and sandstone	6	0.5199
SW	7	−0.1140	Unconsolidated deposits	7	−2.7231
W	8	−0.2686	Sandstone, siltstone, and shale	8	−0.7046
NW	9	−0.2340	Limestone intercalated with shale	9	0.2194
NDVI			Limestone, sandstone, and shale	10	−0.2741
(46, 396.9)	1	0.0010	Limestone and dolomite intercalated with phyllite	11	0.7933
(396.9, 747.8)	2	0.0010	Dolomite, silicalite, phyllite, sandstone, and siltstone	12	1.0446
(747.8, 1098.8)	3	−2.6467	Amphibolite	13	2.0284
(1098.8, 1449.7)	4	−2.5191	Sandstone and siltstone intercalated with slate	14	−0.7046
(1449.7, 1800.6)	5	−1.3168	Sandstone and siltstone interbedded with shale	15	−0.7046
(1800.6, 2151.5)	6	−0.7417	Profile curve		
(2151.5, 2502.4)	7	−0.4388	(−38.6, −28.6)	1	0.9019
(2502.4, 2853.4)	8	0.0010	(−28.6, −18.6)	2	0.9019
(2853.4, 3204.3)	9	0.3448	(−18.6, −8.6)	3	2.0946
(3204.3, 3555.2)	10	0.3301	(−8.6, 2.6)	4	−0.1445
(3555.2, 3906.1)	11	0.0010	(2.6, 12.6)	5	1.3907
(3906.1, 4257.0)	12	0.0010	(12.6, 22.6)	6	2.3735
(4257.0, 4608.0)	13	0.3733	(22.6, 32.6)	7	0.9019
(4608.0, 4958.9)	14	0.3242	(32.6, 44.3)	8	0.9019

Table 4. *Cont.*

Evidence Factors	Classification of Factors	Weight			
(4958.9, 5309.8)	15	0.0010	Curvature		
(5309.8, 5660.7)	16	0.4448	(−87, −71)	1	0.4866
(5660.7, 6011.6)	17	0.2405	(−71, −55)	2	0.4866
(6011.6, 6362.6)	18	0.2123	(−55, −39)	3	0.4866
(6362.6, 6713.5)	19	0.2279	(−39, −23)	4	0.4866
(6713.5, 7064.4)	20	0.0010	(−23, −7)	5	1.5008
(7064.4, 7415.3)	21	0.0010	(−7, 9)	6	−0.0746
(7415.3, 7766.2)	22	−0.2807	(9, 26)	7	1.7797
(7766.2, 8117.2)	23	−0.1889	(26, 42)	8	0.4866
(8117.2, 8468.1)	24	0.1636	(42, 58)	9	0.4866
(8468.1, 8819.0)	25	0.7339	(58, 73)	10	0.4866
Elevation			Land use		
(712.0, 1132.5)	1	2.3614	Garden plot	1	−0.6211
(1132.5, 1553.0)	2	2.5933	Woodland	2	0.2952
(1553.0, 1973.5)	3	2.0378	Land for water bodies and water conservancy facilities	3	−1.2705
(1973.5, 2394.0)	4	1.3316	Grassland	4	1.3025
(2394.0, 2814.5)	5	0.4473	Commercial area	5	1.6173
(2814.5, 3235.0)	6	−0.5438	Land for industrial and mining warehousing	6	−1.2705
(3235.0, 3655.5)	7	−1.7469	Other land	7	−1.2705
(3655.5, 4076.0)	8	−2.8544	Distance to faults		
(4076.0, 4496.5)	9	−4.5328	(0, 17.8)	1	0.7957
(4496.5, 4917.0)	10	−3.5522	(17.8, 35.6)	2	0.1558
(4917.0, 5337.5)	11	−7.4878	(35.6, 53.4)	3	−0.5325
(5337.5, 5758.0)	12	−7.4878	(53.4, 71.2)	4	−0.3549
Slope			(71.2, 89.0)	5	−0.4789
(0, 10)	1	0.0442	(89.0, 106.8)	6	−0.7080
(10, 20)	2	−0.7259	(106.8, 124.6)	7	−1.1509
(20, 30)	3	−0.5053	(124.6, 142.4)	8	−1.7985
(30, 40)	4	0.0442	(142.4, 160.2)	9	−1.3398
(40, 50)	5	0.6464	(160.2, 178)	10	−1.2371
(50, 60)	6	0.9914	(178, 195.8)	11	−1.2571
(60, 70)	7	1.1309	(195.8, 213.6)	12	−1.6333
(70, 80)	8	1.5557	(213.6, 231.4)	13	−2.3612
(80, 90)	9	0.0442	(231.4, 249.2)	14	−3.2262
			(249.2, 267.0)	15	−6.7693

4.3. Landslide Susceptibility Evaluation by WOF-RF Model

4.3.1. Comparison of Rainfall and Seismic Landslide Posteriori Probability Calculation and Zoning

The 407 rainfall and 2936 seismic landslides collected were used as positive samples for the respective models, then a 5 km buffer zone was established with the positive sample points of rainfall and seismic landslides as the center, and the negative samples of the two types of landslides were selected from outside the buffer zone according to the ratio of positive samples:negative samples of 1:1 to form the data set; the data sets of rainfall and

seismic landslides were randomly selected according to 3:1 to form the training set and testing set, and input into the random forest model respectively.

When the number of decision trees are 3000 and 2000, respectively, the errors of rainfall and seismic landslide random forest models tend to stabilize. Based on the average reduction Gini coefficients obtained from the constructed models, the importance ranking of the two influence factors was obtained. The importance of the background factors of rainfall landslides from high to low are as follows: DEM, land use, distance to faults, lithology, profile curve, NDVI, aspect, slope, curvature, and the importance of the background factors of seismic landslides from high to low are as follows: DEM, lithology, distance to faults, slope, land use, NDVI, aspect, curvature, and profile curve.

The rainfall and seismic landslide susceptibility maps obtained based on the WOE-RF model are shown in Figure 4a,b, respectively, and the susceptibility maps of the two types of landslides are divided into five zones, namely, extremely high, high, medium, low, and extremely low based on natural interruption points. The statistical results of the distribution of rainfall and seismic landslides on each zone are shown in Table 5. Figure 4 and Table 5 all show that both rainfall and seismic landslides generally show the trend that the lower the landslide susceptibility level is, the less the known landslides are distributed on it and the larger the proportion of its area of the whole study area.

Table 5. Susceptibility classification and distribution of rainfall and seismic landslides in the upper reaches of Minjiang River Basin.

Landslide Type	Landslide Probability Grading Interval	Landslide Probability Grading Category	Proportion of Known Landslides Corresponding to the Landslide Probability Grading Category	Area Occupied by Landslide Probability Grading Category
Rainfall landslide	[0.9000, 1]	Extremely high	80.34%	6.60%
	[0.4745, 0.9000]	High	15.72%	8.34%
	[0.2588, 0.4745]	Medium	1.97%	10.95%
	[0.0902, 0.2588]	Low	0.74%	22.06%
	[0, 0.0902]	Extremely low	1.23%	52.05%
Seismic landslide	[0.9000, 1]	Extremely high	88.18%	17.13%
	[0.5922, 0.9000]	High	8.62%	9.42%
	[0.3333, 0.5922]	Medium	1.77%	8.28%
	[0.1137, 0.3333]	Low	0.85%	12.58%
	[0, 0.1137]	Extremely low	0.58%	52.59%

Figure 5a,b show extremely high susceptibility areas of rainfall and seismic landslides. Through comparison, it can be found that the similarities between the two are that both extremely high areas of rainfall and seismic landslides are distributed along the main parts and tributaries of rivers; both rainfall and seismic landslides are prone in Maoxian, Lixian, Wenchuanxian, and Dujiangyan, whereas Songpanxian is less prone to landslides compared with the other four counties and cities, especially rainfall landslides; along the line from Xueboding mountain to Lixian, there are relatively few rainfall and seismic landslides in the northwest, while they are mainly concentrated in the southeast area of the upper Minjiang River Basin.

The distribution of the three geological conditions of elevation, land use, and lithology, which are the most important for the evaluation of the susceptibility of rainfall and seismic landslides in extremely high susceptibility areas, were analyzed separately, and the results are shown in Figure 6:

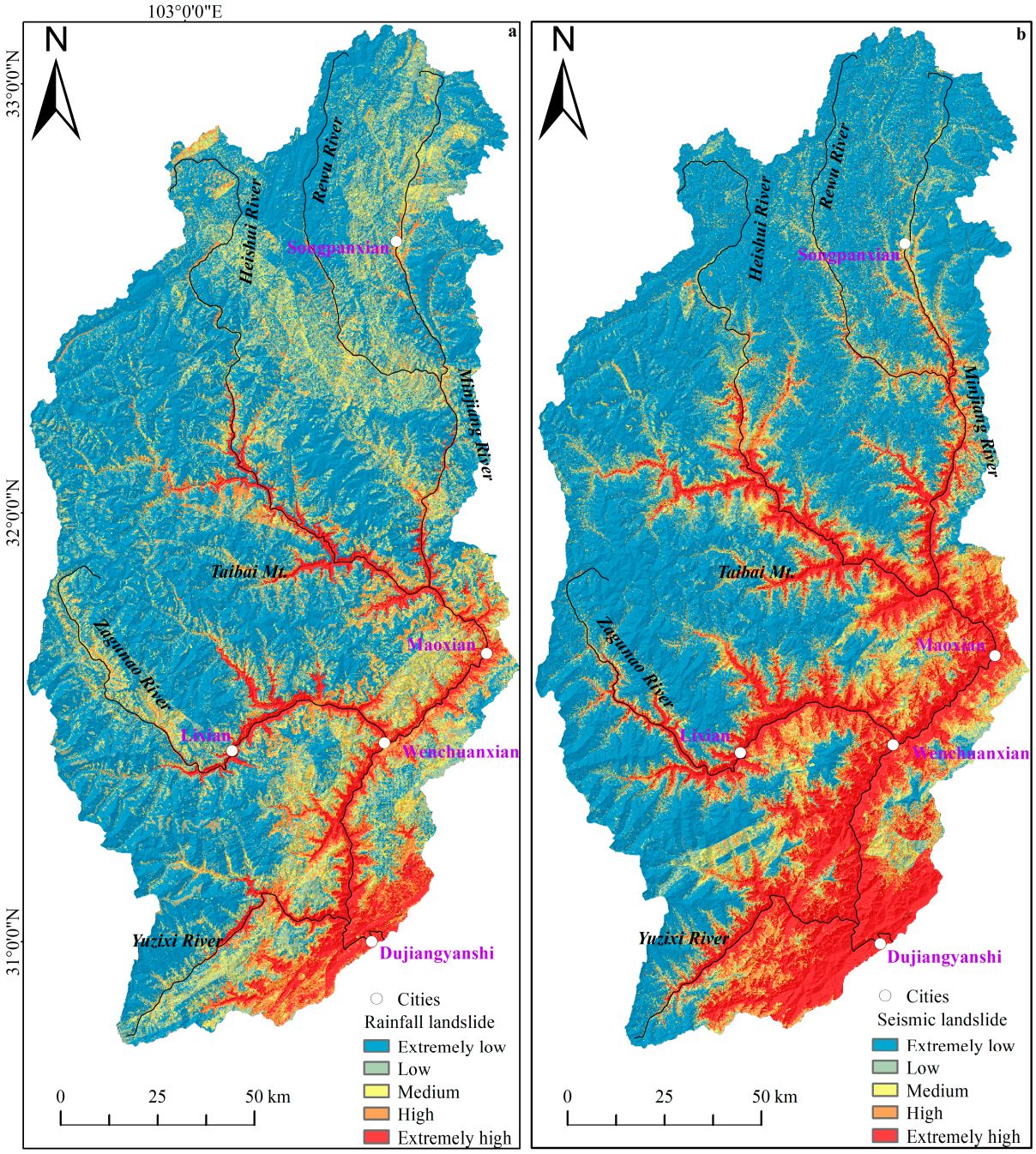

Figure 4. (**a**) Spatial distribution of rainfall landslides in the upper reaches of Minjiang River Basin; (**b**) Spatial distribution of seismic landslides in the upper reaches of Minjiang River Basin.

Figure 6a,b show that the extremely high susceptibility areas of rainfall and seismic landslides are concentrated at the altitudes of 1000–2500 m and 1500–3000 m, respectively, which indicates that the development of seismic landslides is higher than that of rainfall landslides. Figure 6c,d, 1–7 represent Garden plot, Woodland, Land for water bodies and water conservancy facilities, Grassland, Commercial area, Land for industrial and mining warehousing, and Other land, respectively, and Figure 6c,d show that both rainfall and seismic landslides occur easily in Garden plot, Woodland, and Grassland. Figure 6e,f, 1–15 represent Sandstone and siltstone interbedded with phyllite; Shale, phyllite, and siltstone; Granitic rocks; Syenite; Diorite; Limestone and sandstone; Unconsolidated deposits; Sandstone, siltstone, and shale; Limestone intercalated with shale; Limestone, sandstone, and shale; Limestone and dolomite intercalated with phyllite; Dolomite, silicalite, phyllite,

sandstone, and siltstone; Amphibolite; Sandstone and siltstone intercalated with slate; and Sandstone and siltstone interbedded with shale. Figure 6e,f show that both rainfall and seismic landslides are likely to occur in Sandstone and siltstone interbedded with phyllite; Granitic rocks; Limestone and sandstone; Limestone and dolomite intercalated with phyllite; Dolomite, silicalite, phyllite, sandstone, and siltstone; and Amphibolite.

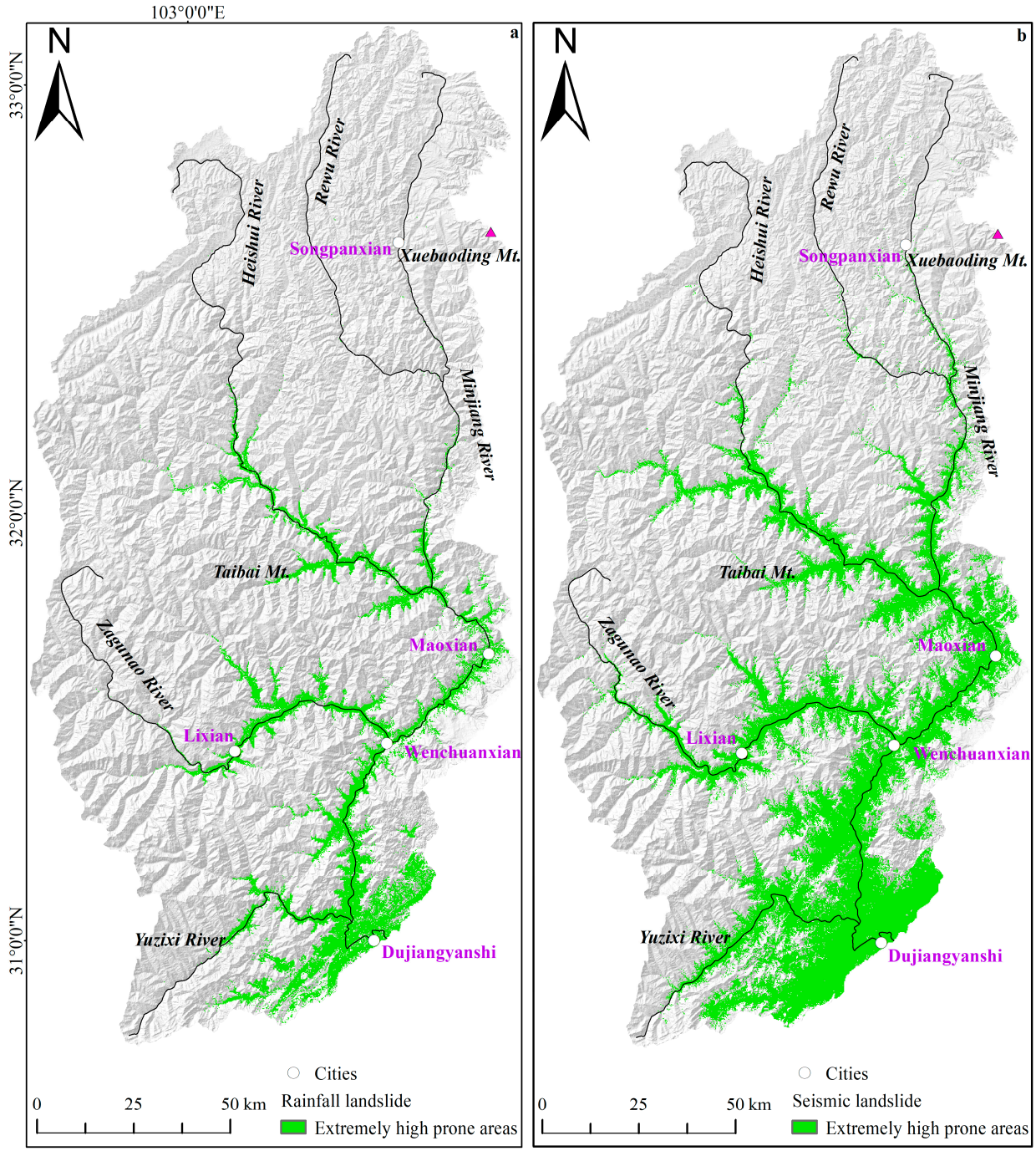

Figure 5. (**a**) Extremely high prone areas of rainfall landslides in the upper reaches of Minjiang River Basin; (**b**) Extremely high prone areas of seismic landslides in the upper reaches of Minjiang River Basin.

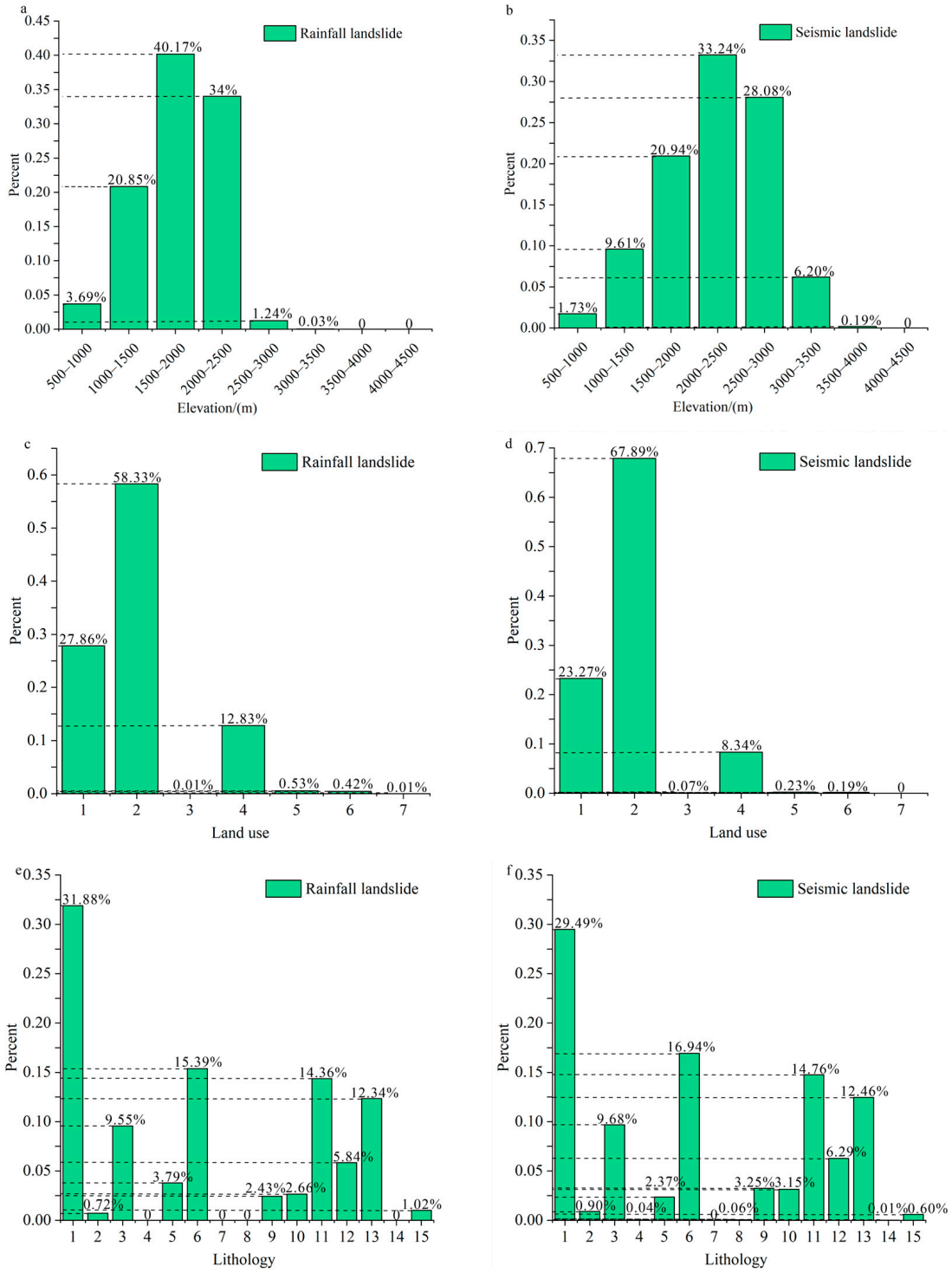

Figure 6. Comparison of distribution of rainfall and seismic landslides that are highly prone to occur in elevation, land use, and lithology ((**a**) Distribution of highly prone areas of rainfall landslide in elevation; (**b**) Distribution of highly prone areas of seismic landslide in elevation; (**c**) Distribution of highly prone areas of rainfall landslide in land use; (**d**) Distribution of highly prone areas of seismic landslide in land use; (**e**) Distribution of highly prone areas of rainfall landslide in lithology; (**f**) Distribution of highly prone areas of seismic landslide in lithology).

4.3.2. Comparison of Landslide Susceptibility Areas from Two Methods

Due to the different ranges of background factors that favor the occurrence of rainfall and seismic landslides, many studies currently do not distinguish the types of landslides

(rainfall-type, seismic-type, or others) when evaluating landslide susceptibility, which may lead to inaccurate results. Therefore, this research attempts to spatially overlay different types of landslide susceptibility maps after distinguishing the types of landslides, and then spatially compare with the landslide susceptibility map without distinguishing the types of landslides in order to see the differences in the distribution of the same class of landslide prone areas between the two.

The collected 3343 landslides of unclassified landslides (after removing landslides distributed in the same grid, 3286 landslides remained) are used as positive samples for the model, a 5 km buffer zone is established with the positive sample points as the center, and the negative samples of landslides are selected from outside the buffer zone in the ratio of positive samples: negative samples of 1:1 to form the data set; then, the unclassified landslide data set is randomly generated in the ratio of 3:1 to form the training set and testing set, and input to the random forest model. When the number of decision trees is 3000, the error of the random forest model tends to be stable. Based on the average reduction Gini coefficient obtained from the constructed model, the importance ranking of the influencing factors obtained from the highest to the lowest are as follows: DEM, lithology, distance to faults, NDVI, slope, land use, aspect, profile curve, and curvature.

The landslide susceptibility map of unclassified landslides obtained based on the WOE-RF model is shown in Figure 7. The landslide susceptibility maps are divided into five classes based on natural interruption points: extremely high, high, medium, low, and extremely low, and the statistical results of landslide distribution on each interval are shown in Table 6.

Table 6. Susceptibility classification and distribution of unclassified landslides in the upper reaches of Minjiang River Basin.

Landslide Type	Landslide Probability Grading Interval	Landslide Probability Grading Category	Proportion of Known Landslides Corresponding to the Landslide Probability Grading Category	Area Occupied by Landslide Probability Grading Category
Unclassified landslide	[0.9000, 1]	Extremely high	87.40%	16.88%
	[0.5882, 0.9000]	High	9.53%	10.24%
	[0.3333, 0.5882]	Medium	1.28%	7.95%
	[0.1137, 0.3333]	Low	1.13%	11.06%
	[0, 0.1137]	Extremely low	0.66%	53.87%
Spatial overlay		Extremely high	89.06%	17.38%
		High	8.23%	11.66%
		Medium	1.61%	12.39%
		Low	0.67%	21.28%
		Extremely low	0.43%	37.29%

Figure 7a shows the landslide susceptibility map of the upper Minjiang River Basin calculated based on the WOE-RF model regardless of landslide type. Figure 7b shows the spatial superposition of the rainfall and seismic landslide susceptibility maps, and classifies (extremely high, extremely high), (extremely high, high), (extremely high, medium), (extremely high, low), (extremely high, extremely low) as extremely high landslide susceptibility zones; (high, high), (high, medium), (high, low), (high, very low) as high landslide susceptibility zones; (medium, medium), (medium, low), (medium, extremely low) as medium landslide susceptibility zones; (low, low), (low, extremely low) as low landslide susceptibility zones; and (extremely low, extremely low) as extremely low landslide susceptibility zones [32].

The statistical information on the landslide susceptibility zones in the upper reaches of the Minjiang River Basin obtained by the two methods is shown in Table 6, both of which show that the higher the grade of the landslide susceptibility zone, the more the number of known landslides falling into the zone. The difference in the proportion of

known landslides in the corresponding susceptibility zones to all known landslides is 1.66%, 1.3%, 0.33%, 0.46%, and 0.23%, respectively, all within 2%; the difference in the ratio of each landslide susceptibility zone to all known landslides is 0.5%, 1.42%, 4.44%, 10.22%, 16.58%, respectively; the overlapping areas of the corresponding susceptibility intervals were superimposed and found to be 84.91%, 48.20%, 39.39%, 44.84%, and 65.44% for extremely high, high, medium, low, and extremely low, respectively.

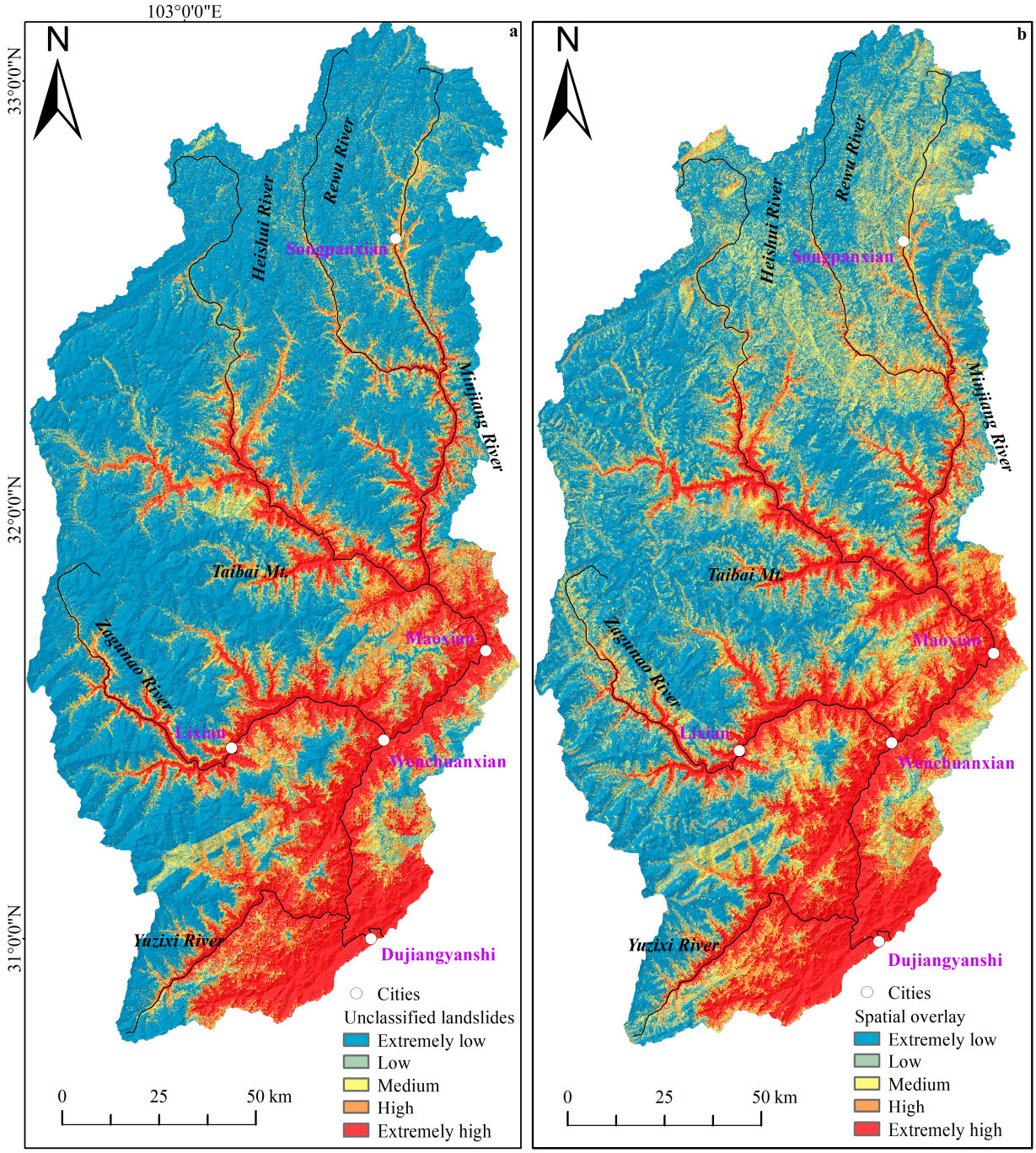

Figure 7. Zoning map of unclassified landslide susceptibility in the upper reaches of Minjiang River Basin ((**a**) Unclassified landslides susceptibility map; (**b**) Spatial overlay landslides susceptibility map).

The results of the landslide susceptibility assessment obtained using spatial superposition and unclassified landslides are compared by using proportional statistics, and the

results are shown in Figure 8. The solid line shows the distribution of different grades of landslide susceptibility obtained by using the unclassified landslides, and the dashed line shows the distribution of different grades of landslide susceptibility obtained using the spatial superposition of rainfall and seismic landslide susceptibility maps.

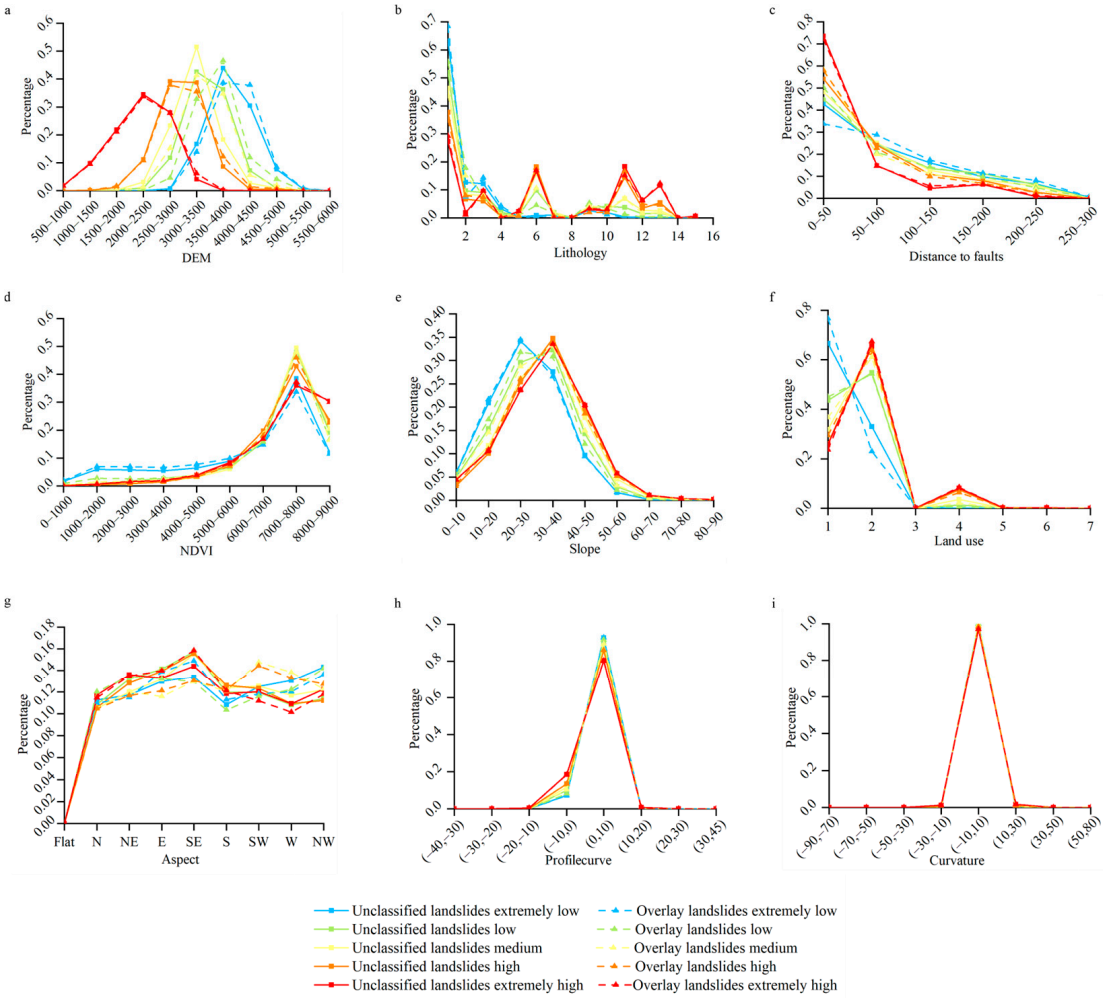

Figure 8. Predicted distribution results of different landslide susceptibility classes on background factors ((**a**) Distribution on elevation; (**b**) Distribution on lithology; (**c**) Distribution on distance to faults; (**d**) Distribution on NDVI; (**e**) Distribution on slope; (**f**) Distribution on land use; (**g**) Distribution on aspect; (**h**) Distribution on profile curve; (**i**) Distribution on curvature).

Figure 8a–i show the distribution of both in terms of elevation, lithology, distance to faults, NDVI, slope, land use, aspect, profile curve, and curvature, respectively.

There are the same results between the two resources of landslide susceptibility: for the elevation factor, the predicted landslide areas for extremely low, low, medium, high, and extremely high grades are concentrated in (3500, 4500), (3000, 4000), (2500, 4000), (2500, 3500), and (1500, 3000) for both. For the lithology factor, extremely low, low, medium, high, and extremely high grades are concentrated in Sandstone and siltstone interbedded with phyllite, Granitic rocks; Sandstone and siltstone interbedded with phyllite; Sandstone and siltstone interbedded with phyllite, limestone, and sandstone; Sandstone, and siltstone interbedded with phyllite, limestone and sandstone, and limestone and dolomite intercalated with phyllite; Sandstone and siltstone interbedded with phyllite, limestone and sandstone, limestone and dolomite intercalated with phyllite, and Amphibolite; they are all concentrated in Sandstone and siltstone interbedded with phyllite. As for the fault factor, extremely low-, low-, medium- and high-grade landslide prediction areas are mainly

concentrated in (0, 150), which means (0, 30,000) m, and extremely high-grade areas are concentrated in (0, 100), which means (0, 20,000) m. For the NDVI factor, extremely low-, low-, medium-, high-, and extremely high-grade landslide prediction areas are mainly distributed in (6000, 9000). For slope factor, extremely low- and low-grade landslide prediction areas are mainly distributed in (10, 40), and medium, high, and extremely high grade are mainly distributed in (10, 50). For the land use factor, extremely low-, low-, medium-, high-, and extremely high-grade landslide prediction areas are mainly distributed in Garden plot and Woodland. For the aspect factor, except for the plane direction, the distributions of extremely low, low, medium, high and extremely high landslide prediction areas are not much different in each slope direction, and the distribution is relatively uniform. For the profile curve and curvature factor, extremely low, low, medium, high, and extremely high landslide prediction areas are all concentrated in (–10, 10).

There are also the different results between the two resources of landslide susceptibility: a 10% difference was used as a threshold to determine whether the difference between the two was too large, and it was found that the difference among the distributions of each classification in lithology, NDVI, slope, aspect, profile curve, and curvature were all within 10%. For the elevation factor, the low gradation of both (unclassified landslides susceptibility, spatially superimposed landslide susceptibility) on (500, 1000), (1000, 1500), (1500, 2000), (2000, 2500), (2500, 3000), (3000, 3500), (3500, 4000), (4000, 4500), (4500, 5000), (5000, 5500), (5500, 6000) are 0, 0.03%, 0.36%, 0.85%, 11.79%, 42.65%, 36.27%, 7.18%, 0.77%, 0.10%, 0; 0, 0, 0, 0, 0.11%, 4.51%, 32.85%, 46.52%, 11.88%, 4.05%, 0.08%, and 0; the difference between the two in the range (3500, 4000) is more than 10%. The medium grading on each interval are 0, 0, 0.17%, 3.03%, 23.30%, 51.54%, 18.24%, 2.72%, 0.93%, 0.07%, 0; 0, 0.01%, 0.08%, 1.31%, 15.22%, 41.30%, 34.65%, 5.53%, 1.85%, 0.05%, and 0, and the difference between the two is more than 10% in the range of (3000, 3500), (3500, 4000). For the distance to faults factor, the medium grading of both (unclassified landslide susceptibility, spatially superimposed landslide susceptibility) on (0, 20), (50, 100), (100, 150), (150, 200), (200, 250), (250, 300) are 48.12%, 25.15%, 12.69%, 8.39%, 5.64%, 0.01%; 58.30%, 19.96%, 11.20%, 6.53%, 3.94%, and 0.08%, and the difference between the two in the range of (0, 50) (within (0, 10,000) meters) is more than 10%. For the land use factor, the low grading of both (unclassified landslide susceptibility, spatially superimposed landslide susceptibility) on Garden plot, Woodland, Land for water bodies and water conservancy facilities, Grassland, Commercial area Land for industrial and mining warehousing, and Other land are 66.58%, 32.96%, 0.27%, 0.14%, 0.05%, 0, 0; 76.63%, 22.93%, 0.35%, 0.06%, 0.02%, 0, 0, 0, and both on Garden plot and Woodland differ by more than 10%.

4.3.3. WOF-RF Model Accuracy Evaluation

(1) Confusion matrix

Based on the confusion matrix and calculated from Table 7, the accuracy, recall of rainfall, and seismic and unclassified landslides can be calculated separately, as shown in Table 8:

As can be seen from Table 8, the accuracy of rainfall, seismic and unclassified landslide dataset are above 80%; meanwhile, except for the lower recall rate of the rainfall landslide test set, all the others are above 80%, although the recall rate of rainfall landslide testing set is lower, and the recall rate of the whole dataset of the rainfall landslide is above 90%, so both the accuracy and recall rate show that the accuracy of the model is high.

(2) ROC curve

Figure 9a,b, and c show the ROC curves of rainfall, seismic, and unclassified landslides, respectively. Figure 9a shows that the AUC areas of the rainfall landslide training set, testing set, and the whole data set are 0.9997, 0.9485, and 0.9547, respectively. Figure 9b shows that the AUC areas of the seismic landslide training set, testing set, and the whole data set are 0.9996, 0.9809, and 0.9211, respectively. Figure 9c shows that the AUC areas of the unclassified landslide training set, testing set, and the whole data set are 0.9997, 0.9822, and

0.9207, respectively. It can be seen that the WOE-RF model has a high evaluation accuracy for all three landslide datasets.

Table 7. Confusion matrix of rainfall, seismic, unclassified landslides' training set, testing set, and the whole data set.

	Reality \ Prediction	0	1
Rainfall landslide training set	0	306	47
	1	0	259
Rainfall landslide testing set	0	100	33
	1	1	68
Rainfall landslide whole set	0	468,447	39
	1	94,661	368
Seismic landslide training set	0	2202	221
	1	0	1981
Seismic landslide testing set	0	724	127
	1	10	607
Seismic landslide whole set	0	466,625	486
	1	93,954	2450
Unclassified landslide training set	0	2466	273
	1	0	2192
Unclassified landslide testing set	0	813	143
	1	8	678
Unclassified landslide whole set	0	467,927	559
	1	92,302	2727

Table 8. Accuracy, recall of rainfall, seismic, unclassified landslides' training set, testing set, and the whole data set.

	Accuracy	Recall
Rainfall landslide training set	0.9232	0.8464
Rainfall landslide testing set	0.8317	0.6733
Rainfall landslide whole set	0.8319	0.9042
Seismic landslide training set	0.9498	0.8996
Seismic landslide testing set	0.9067	0.8270
Seismic landslide whole set	0.8324	0.8345
Unclassified landslide training set	0.9446	0.8892
Unclassified landslide testing set	0.9080	0.8258
Unclassified landslide whole set	0.8352	0.8299

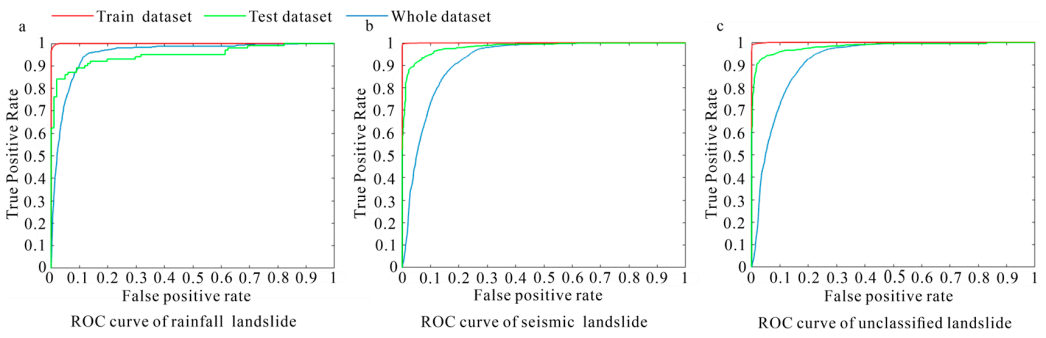

Figure 9. (**a**) ROC curve of rainfall landslide in the upper reaches of Minjiang River Basin; (**b**) ROC curve of seismic landslide in the upper reaches of Minjiang River Basin; (**c**) ROC curve of unclassified landslide in the upper reaches of Minjiang River Basin.

5. Discussion

5.1. Comparison of Rainfall and Seismic Landslide Susceptibility in the Upper Reaches of Minjiang River Basin

The importance ranking of the factors for evaluating the susceptibility of rainfall landslides in the upper reaches of Minjiang River Basin is as follows: DEM, land use, distance to faults, lithology, profile curve, NDVI, aspect, slope, and curvature. The importance ranking of the factors for evaluating the susceptibility of seismic landslides in the upper reaches of Minjiang River Basin is as follows: DEM, lithology, distance to faults, slope, land use, NDVI, aspect, curvature, and profile curve. In terms of the ranking of the importance of factors, DEM has the greatest influence on the development of rainfall and seismic landslides, indicating that unstable slope movement develops at a specific elevation location; in addition, land use and lithology are the second most important factors affecting rainfall and seismic landslides, respectively; the distance to faults is the third most important factor affecting rainfall and seismic landslides. Seismic landslides are commonly found in places close to the faults, and the reason why faults have a greater influence on rainfall landslides in this study may be that unstable activities at faults provide a potential source of material for rainfall, and therefore shallow rainfall landslides are likely to occur when rainfall occurs. However, the specific causes need to be analyzed in depth in the context of the complex geology of the upper Minjiang River Basin. By comparing the two susceptibility maps, it was found that the areas with high susceptibility levels are roughly distributed along the rivers in terms of spatial distribution, and the southeast direction of the line from Xuebaoding mountain to Lixian is the high landslide occurrence area for both. The extremely high susceptibility areas of the two were extracted separately and their distributions in DEM, land use, and lithology factors were analyzed. It was found that the differences between the distributions of the two in terms of land use and lithology are small, and seismic landslides are more likely to occur at a height of 1500–3000 m, while rainfall landslides are more likely to occur at a height of 1000–2500 m. This may be related to the triggering principles of the two, with most seismic landslides being bedrock landslides and most rainfall landslides being shallow landslides; meanwhile, this is also consistent with the conclusion that "rainfall landslides are more likely to occur at lower slopes, while earthquake landslides are more likely to occur at steeper slopes" in the upper reaches of Minjiang River Basin, obtained using a statistical method of landslide proportion by Bai et al. [41]. Therefore, from the above results, it is clear that we cannot simply regard different types of landslides as the same when conducting detailed studies.

5.2. Comparison of Two Mapping Methods for Landslide Susceptibility in the Upper Minjiang River Basin

The two methods of obtaining landslide susceptibility in the upper reaches of the Minjiang River Basin do not differ greatly in terms of the distribution of known landslides on each susceptibility interval and the proportion of area occupied by each susceptibility interval when directly performing machine learning on unclassified landslides, as well as spatial stacking on the susceptibility of rainfall and seismic landslides. However, when the spatial superposition of the two methods was carried out, it was found that extremely high and extremely low susceptibility zones had 84.91% and 65.44% overlap, respectively, while the other three susceptibility zones did not overlap by more than 50%, indicating that the prediction results of the two methods are different. At the same time, statistical analysis was done on the distribution of both corresponding landslide prediction grading areas in terms of background factors. The differences in the distribution of predicted results in terms of lithology, NDVI, slope, aspect, profile curve, and curvature are within 10%, but the differences in the distribution of both low and medium landslide prediction grading areas in terms of elevation are larger; the differences in the distribution of medium-graded landslide prediction areas in terms of distance to faults are larger; the differences in the distribution of low-graded landslide prediction areas in terms of land use are larger.

The reasons for the differences are speculated as follows: for unclassified landslides composed of rainfall and seismic landslides, the spatial relationship between the two types of landslides and the background factors affecting the landslide development is considered at the same time. Whether from the calculation of weight or the machine learning algorithm of random forest, it is equivalent to taking the union of the results that are conducive to both rainfall landslides and seismic landslides. For the landslide susceptibility map generated by spatial stacking of rainfall and seismic landslide susceptibility maps, the initial consideration was given to the demand for background factors for different types of landslides, as the development of different types of landslides requires different requirements for background factors. At the same time, the final landslide susceptibility level determined by stacking is based on the maximum susceptibility interval of different types of landslides before stacking. From this perspective, in fact, there have been differences since the initial calculation of weights that express the spatial relationship between landslides and factors. Considering the types of landslides, the spatial relationships between rainfall, seismic landslides, and background factors were obtained, and the same background factor was given different weights, respectively, when machine learning was conducted. The relationship between the two types of landslides and background factors was also considered separately. When not considering the type of landslides, the weight of the obtained factors took into account rainfall and seismic landslides at the same time, and the same factor only had one weight that expresses the relationship between all landslides and factors, which also affected the subsequent calculation of machine learning. When conducting machine learning algorithms simultaneously, the situation where two types of landslides coexist was also considered. Based on the above analysis, it can be determined that there may be significant differences between the landslide susceptibility obtained using the spatial stacking of rainfall and seismic landslide susceptibility maps and the susceptibility results obtained directly using unclassified landslides.

It can be seen that not every scenario can be considered without the type of landslide. For the assessment of landslide susceptibility, it is necessary to separate different types of landslides when the needs for landslide background factors are not exactly the same for both types of landslides. All in all, it is essential to judge whether the different types of landslides need to be viewed separately for different problem scenarios and to solve the detailed problems.

5.3. Limitations and Prospects

The factors affecting the occurrence of landslides can be divided into background factors and triggering factors; this research is based on using the background factors affecting the occurrence of landslides to evaluate the spatial susceptibility of rainfall and seismic landslides in the upper reaches of the Minjiang River Basin. However, the role of trigger factors cannot be ignored. Based on this research, rainfall factors should be considered for inclusion in the study of rainfall landslides, and peak ground acceleration factor should be considered for inclusion in the study of seismic landslides.

In addition, in the susceptibility mapping of landslides in the upper reaches of the Minjiang River Basin, it was found that the landslide susceptibility maps obtained using the spatial superposition of rainfall and seismic landslide susceptibility maps differed significantly from those obtained directly from unclassified landslides, which on the one hand illustrates the necessity of classifying landslides for specific problems. At the same time, the respective weights of the two landslide susceptibility layers were not considered when the spatial overlay was conducted, and the distribution of the two different types of landslides in terms of each geological factor shows that they have different needs for background factors. In addition, the changes in weights due to the frequency of landslide occurrences of both can be considered in the spatial overlay of the two in the future.

6. Conclusions

This research takes the upper reaches of the Minjiang River Basin as the study area and evaluates the susceptibility of rainfall, seismic, and unclassified landslides based on WOE-RF. Then, a spatial comparison of landslide susceptibility maps in the upper reaches of the Minjiang River Basin, obtained by overlaying landslide susceptibility maps from rainfall and earthquake landslides and directly from unclassified landslides, was conducted:

(1) In terms of model construction, the event impact factors entered into the machine learning model in previous studies are often assigned weights by the expert scoring method, AHP, and other biased subjective methods. In this research, we used a purely data-driven weight of evidence method without human intervention to assign corresponding weights to each factor to participate in the calculation of the model, and the factor weights obtained from weight of evidence are the expression of the spatial relationship between landslides and the factors influencing the occurrence of the landslides, which can reduce the redundancy of the data input to the machine learning model to a certain extent.

(2) In terms of spatial location distribution, rainfall and seismic landslides have the following points in common: they are prone to occur along rivers; landslides are more likely to occur in Maoxian, Lixian, Wenchuanxian, and Dujiangyancity, while landslides are less likely to occur in Songpanxian; and landslides are more likely to occur in the southeast of the line from Xuebaoding to Lixian. In terms of the distribution of geological factors, seismic landslides are distributed at a slightly higher elevation than rainfall landslides, whilst land use and lithological conditions in both susceptible areas are similar.

(3) The differences between the landslide susceptibility maps obtained by superimposing rainfall and seismic landslide susceptibility maps and the result obtained by directly using unclassified landslides are large, which is mainly caused by the difference in the principles of the two mapping methods and shows that it is important to see whether it is necessary to differentiate the types of landslides for solving the problems in different contexts.

(4) The accuracy of the rainfall, seismic, and unclassified landslide models calculated from the confusion matrix are all above 80%, and the AUC area is greater than 0.9, both of which indicate the high accuracy of the WOE-RF model.

Author Contributions: Conceptualization, X.W. and S.B.; Methodology, X.W. and S.B.; Software, X.W.; Validation, X.W.; Formal analysis, X.W.; Investigation, X.W. and S.B.; Resources, S.B.; Data curation, X.W. and S.B.; Writing—original draft preparation, X.W.; Writing—review and editing, X.W. and S.B.; Visualization, X.W.; Supervision, S.B.; Project administration, S.B.; Funding acquisition, S.B. All authors have read and agreed to the published version of the manuscript.

Funding: This study were supported by the National Natural Science Foundation of China (grant nos. 41941017 and 41877522) and Youth innovation promotion association CAS 2022378.

Data Availability Statement: Not applicable.

Conflicts of Interest: The authors declare no conflict of interest.

References

1. Bai, S.B.; Wang, J.; Zhang, Z.G.; Cheng, C. Combined landslide susceptibility mapping after Wenchuan earthquake at the Zhouqu Segment in the Bailongjiang Basin, China. *Catena* **2012**, *99*, 18–25. [CrossRef]
2. Chang-Jo, F.C.; Andrea, G.F. Probabilistic prediction models for landslide hazard mapping. *Photogramm. Eng. Remote Sens. J. Am. Soc. Photogramm.* **1999**, *65*, 1389–1399.
3. Shi, J.S.; Shi, L.; Wu, S.R.; Wang, T. Difficulties and countermeasures in the practice of landslide risk assessment. *Geol. Bull. China* **2009**, *28*, 1020–1030. (In Chinese with English Abstract)
4. Agterberg, F.P. Computer programs for mineral exploration. *Science* **1989**, *245*, 76–81. [CrossRef] [PubMed]
5. Agterberg, F.P.; Bonham-Carter, G.F.; Wright, D.F. Statistical pattern integration for mineral exploration. *Comput. Appl. Resour. Estim.* **1990**, 1–21. [CrossRef]

6. Fan, D.L.; Cui, X.M.; Yuan, D.B.; Wang, J.F.; Yang, J.L.; Wang, S.Y. Weight of evidence method and its applications and development. *Procedia Environ. Sci.* **2011**, *11*, 1412–1418. [CrossRef]
7. Dahal, R.K.; Hasegawa, S.; Nonomura, A.; Yamanaka, M.; Masuda, T.; Nishino, K. GIS-based weights-of-evidence modelling of rainfall-induced landslides in small catchments for landslide susceptibility mapping. *Environ. Geol.* **2008**, *54*, 311–324. [CrossRef]
8. Sadisun, I.A.; Telaumbanua, J.A.; Kartiko, R.D.; Dinata, I.A. Weight of evidence method for landslide susceptibility mapping in Sigi Biromaru, central Sulawesi. *IOP Conf. Ser. Earth Environ. Sci.* **2021**, *830*, 12026–12029. [CrossRef]
9. Yang, H.Y.; Xu, X.N.; Yang, H.F. Risk assessment of earthquake-triggered landslides in Jiuzhaigou Valley based on weight of evidence. *Chin. J. Geol. Hazard Control* **2020**, *31*, 20–29. (In Chinese with English Abstract)
10. Hu, Y.; Li, D.Y.; Meng, S.S.; Sun, Y.Q. Evaluation of landslide susceptibility in Badong county based on weight of evidence. *Bull. Geol. Sci. Technol.* **2020**, *39*, 187–194. (In Chinese with English Abstract)
11. Cheng, Q.M.; Agterberg, F.P. Fuzzy weights of evidence method and its application in mineral potential mapping. *Nat. Resour. Res.* **1999**, *8*, 27–35. [CrossRef]
12. Huang, H.F.; Yao, S.J.; Ding, Z.J. Application of GIS-based weight of evidence in ore formation prediction—A case Study of gold ore prediction in Minxian-Lixian area of Gansu province. *Bull. Geol. Sci. Technol.* **2003**, *22*, 77–82. (In Chinese with English Abstract)
13. Bai, S.B.; Lü, G.N.; Wang, J.; Zhou, P.G.; Ding, L. GIS-based rare events logistic regression for landslide-susceptibility mapping of Lianyungang, China. *Environ. Earth Sci.* **2011**, *62*, 139–149. [CrossRef]
14. Mao, Y.M.; Zhang, M.X.; Cheng, X.J.; Peng, Z. Landslide hazard evaluation based on uncertain Bayesian classification technique. *J. China Univ. Min. Technol.* **2015**, *44*, 769–774. (In Chinese with English Abstract)
15. Wang, Q.; Xue, Y.; Zhang, W.; Long, Y.H.; Zhou, S.L. Landslide susceptibility evaluation based on support vector machine. *J. Hunan City Coll. Nat. Sci. Ed.* **2021**, *30*, 22–28. (In Chinese with English Abstract)
16. Li, T.; Tian, Y.; Wu, L.; Liu, L. Landslide hazard zoning based on random forest method. *Geogr. Geo-Inf. Sci.* **2014**, *30*, 25–30. (In Chinese with English Abstract)
17. Yang, S.; Li, D.Y.; Yan, L.X.; Huang, Y.; Wang, M.Z. Evaluation of landslide geological hazard susceptibility of high and steep bank slopes of Wujiang River based on random forest model. *Saf. Environ. Eng.* **2021**, *28*, 131–138. (In Chinese with English Abstract)
18. Wu, X.Q.; Lai, C.G.; Chen, X.H.; Ren, X.W. Landslide hazard evaluation based on random forest weights: An example from the Dongjiang River Basin. *J. Nat. Disasters* **2017**, *26*, 119–129. (In Chinese with English Abstract)
19. Liu, J.; Li, S.L.; Chen, T. Landslide susceptibility evaluation based on optimized random forest model. *Geomat. Inf. Sci. Wuhan Univ.* **2018**, *43*, 1085–1091. (In Chinese with English Abstract)
20. Mandal, K.; Saha, S.; Mandal, S. Applying deep learning and benchmark machine learning algorithms for landslide susceptibility modelling in Rorachu river basin of Sikkim Himalaya, India. *Geosci. Front.* **2021**, *12*, 101203. [CrossRef]
21. Wang, D.; Yang, R.H.; Wang, X.; Li, S.D.; Tan, J.X.; Zhang, S.Q.; Wei, S.Y.; Wu, Z.Y.; Chen, C.; Yang, X.X. Evaluation of deep learning algorithms for landslide susceptibility mapping in an alpine-gorge area: A case study in Jiuzhaigou County. *J. Mt. Sci.* **2023**, *20*, 484–500. [CrossRef]
22. Arabameri, A.; Pradhan, B.; Rezaei, K.; Sohrabi, M.; Kalantari, Z. GIS-based landslide susceptibility mapping using numerical risk factor bivariate model and its ensemble with linear multivariate regression and boosted regression tree algorithms. *J. Mt. Sci.* **2019**, *16*, 595–618. [CrossRef]
23. PourghasemI, H.R.; Gayen, A.; Panahi, M.; Rezaie, F.; Blaschke, T. Multi-hazard probability assessment and mapping in Iran. *Sci. Total Environ.* **2019**, *692*, 556–571. [CrossRef] [PubMed]
24. Guo, Z.Z.; Yin, K.L.; Fu, S.; Huang, F.M.; Gui, L.; Xia, H. Landslide susceptibility evaluation based on GIS and WOE-BP model. *Earth Sci.* **2019**, *44*, 4299–4312. (In Chinese with English Abstract)
25. Li, Y.J.; Hu, Q.C.; Liu, H.Z.; Du, Z.; Chen, J.W.; Huang, J.C.; Huang, F.M. Landslide susceptibility evaluation with coupled informativeness and logistic regression model. *Yangtze River* **2021**, *52*, 95–102. (In Chinese with English Abstract)
26. Ma, X.; Wang, N.Q.; Li, X.K.; Yan, D.; Li, J.L. Evaluation of landslide susceptibility based on RF-FR model--Lueyang county as an example. *Northwestern Geol.* **2022**, *55*, 335–344. (In Chinese with English Abstract)
27. Bai, Z.G.; Liu, Q.M.; Liu, Y. Landslide susceptibility evaluation based on entropy index and random forest model. *Yangtze River* **2022**, *53*, 95–102. (In Chinese with English Abstract)
28. Araya-Munoz, D.; Metzger, M.J.; Stuart, N.; Wilson, A.; Carvajal, D. A spatial fuzzy logic approach to urban multi-hazard impact assessment in Concepción, Chile. *Sci. Total Environ.* **2017**, *576*, 508–519. [CrossRef]
29. Bathrellos, G.D.; Skilodimou, H.D.; Chousianitis, K.; Youssef, A.M.; Pradhan, B. Suitability estimation for urban development using multi-hazard assessment map. *Sci. Total Environ.* **2017**, *575*, 119–134. [CrossRef]
30. Furlan, E.; Torresan, S.; Critto, A.; Marcomini, A. Spatially explicit risk approach for multi-hazard assessment and management in marine environment: The case study of the Adriatic Sea. *Sci. Total Environ.* **2018**, *618*, 1008–1023. [CrossRef]
31. Hagenlocher, M.; Renaud, F.G.; Haas, S.; Sebesvari, Z. Vulnerability and risk of deltaic social-ecological systems exposed to multiple hazards. *Sci. Total Environ.* **2018**, *631–632*, 71–80. [CrossRef] [PubMed]
32. Thierry, P.; Stieltjes, L.; Kouokam, E.; Nguéya, P.; Salley, P.M. Multi-hazard risk mapping and assessment on an active volcano: The GRINP project at Mount Cameroon. *Nat. Hazards* **2008**, *45*, 429–456. [CrossRef]

33. Mahendra, R.S.; Mohanty, P.C.; Bisoyi, H.; Kumar, T.S.; Nayak, S. Assessment and management of coastal multi-hazard vulnerability along the Cuddalore–Villupuram, east coast of India using geospatial techniques. *Ocean Coast. Manag.* **2011**, *54*, 302–311. [CrossRef]
34. Ke, C.Y.; He, S.; Qin, Y.G. Comparison of natural breaks method and frequency ratio dividing attribute intervals for landslide susceptibility mapping. *Bull. Eng. Geol. Environ.* **2023**, *82*, 384. [CrossRef]
35. Wang, H.F.; Meng, Y.; Wang, H.L.; Wu, Z.N.; Guan, X.J. The application of integrating comprehensive evaluation and clustering algorithms weighted by maximal information coefficient for urban flood susceptibility. *J. Environ. Manag.* **2023**, *344*, 118846. [CrossRef]
36. Shi, C.J.; Zhang, F.Q. A forest fire susceptibility modeling approach based on integration machine learning algorithm. *Forests* **2023**, *14*, 1506. [CrossRef]
37. Wang, W.F.; Geng, Y.; Wang, Q.Z.; Shan, J.X.; Chen, X.L. Experimental study of rainfall and seismic landslides. *Seismol. Geol.* **2012**, *34*, 810–819. (In Chinese with English Abstract)
38. Ding, J.H. Study on the Formation Mechanism and Dynamic Model of Landslide by Earthquake and Rainfall. Master's Thesis, Fuzhou University, Fuzhou, China, 2013. (In Chinese with English Abstract).
39. Bai, S.B.; Cheng, C.; Wang, J.; Thiebes, B.; Zhang, Z.G. Regional scale rainfall- and earthquake-triggered landslide susceptibility assessment in Wudu county, China. *J. Mt. Sci.* **2013**, *10*, 743–753. [CrossRef]
40. Kappes, M.S.; Keiler, M.; von Elverfeldt, K.; Glade, T. Challenges of analyzing multi-hazard risk: A review. *Nat. Hazards* **2012**, *64*, 1925–1958. [CrossRef]
41. Bai, S.B.; Lu, P.; Thiebes, B. Comparing characteristics of rainfall- and earthquake-triggered landslides in the upper Minjiang Catchment, China. *Eng. Geol.* **2020**, *268*, 105518. [CrossRef]
42. Chang, X.J.; Ding, J.; Wei, L.W.; Wang, D.W.; Mao, Y.; Yan, Y. A preliminary investigation on the distribution pattern of geological hazard development in the upper reaches of Minjiang River. *Sediment. Geol. Tethyan Geol.* **2007**, *27*, 103–108. (In Chinese with English Abstract)
43. Lu, P.; Han, J.P.; Hao, T.; Li, R.X.; Qiao, G. Seasonal deformation of permafrost in Wudaoliang Basin in Qinghai-Tibet Plateau revealed by StaMPS-InSAR. *Mar. Geod.* **2019**, *43*, 1–20. [CrossRef]
44. Xu, X.L. 30 m Year-by-Year NDVI Maximum Dataset in China. Resource and Environmental Science Data Registration and Publication System. (In Chinese with English Abstract). Available online: https://www.resdc.cn/ (accessed on 1 October 2022).
45. Bonham-Carter, G.F. *Geographic Information Systems for Geoscientists: Modelling with GIS*; Elsevier: Amsterdam, The Netherlands, 1994; pp. 302–329.
46. Li, Y.W.; Zhao, J.M.; Li, C.Y. *Potential Mineral Resource Evaluation Methods Based on GMS, DSS and GIS (Previous)*; Seismological Press: Beijing, China, 2007; (In Chinese with English Abstract).
47. Breiman, L. Random forests. *Mach. Learn.* **2001**, *45*, 5–32. [CrossRef]
48. Li, H. *Statistical Learning Methods*; Tsinghua University Press: Beijing, China, 2012; pp. 55–63. (In Chinese with English Abstract)
49. Loomis, J.M. Analysis of Tactile and Visual Confusion Matrices. *Percept. Psychophys.* **1982**, *31*, 41–52. [CrossRef] [PubMed]
50. Cantarino, I.; Carrion, M.A.; Goerlich, F.; Ibañez, V.M. A ROC analysis-based classification method for landslide susceptibility maps. *Landslides* **2018**, *16*, 265–282. [CrossRef]
51. Ye, C.M.; Wei, R.L.; Ge, Y.G.; Li, Y.; José, M.J.; Jonathan, L. GIS-based spatial prediction of landslide using road factors and random forest for Sichuan-Tibet Highway. *J. Mt. Sci.* **2022**, *19*, 461–476. [CrossRef]
52. Jin, Y.J. *Statistics*; China Renmin University Press: Beijing, China, 2010. (In Chinese with English Abstract)